somewhat less than that contributed by the atmosphere and antenna system (~100 K) and with a bandwidth as large as a few megahertz allows something close to optimum system performance obtainable from the earth's surface.

A further criterion is important to an amplifier and antenna system if it is to be used on an interferometer involving two or more antennas, i.e., for techniques generally known as long baseline interferometry, or aperture systhesis. Such systems have yielded remarkably high angular resolution on a variety of astronomical objects, for which baselines as long as intercontinental distances are sometimes used. To obtain accuracy in position rather than resolution alone, an interferometer must have its two antennas connected by a microwave line of fixed or determinable length, so that the relative phase of the partial wave received in the two or more antennas can be accurately known. Hence the additional property of antenna–receiver systems for radio astronomy, or of a sensitive amplifier used with such a system, is the stability of the phase relation between its input and output.

The large number of molecular resonances that have recently been detected and measured with some precision in the millimeter range have yielded much interesting astronomical information. But, as may be expected, the fruitfulness of this work uncovers further frontiers which demand still more extended and exacting measurements. For the moment, these demands for shorter wavelengths, more sensitivity, more directionality, and relatively precise measurements of power and frequency are probably greater than is immediately needed for most other purposes. However, their development can be expected to be rewarding both for astronomy and for other scientific experiments which become practical as new possibilities are made available. Perhaps somewhat later, but almost certainly somewhere in the future, we may also expect from them a variety of new technological and commercial applications.

K-Band Traveling-Wave Maser Using Ruby

K. SIGFRID YNGVESSON, MEMBER, IEEE, ALBERT C. CHEUNG, MICHAEL F. CHUI, APOSTLE G. CARDIASMENOS, MEMBER, IEEE, SHIH-YUAN WANG, MEMBER, IEEE, AND CHARLES H. TOWNES, FELLOW, IEEE

Abstract—**A *K*-band ruby traveling-wave maser (TWM) has been developed, which has provided a decrease in system noise temperature compared to other front ends presently used in radio telescopes at *K*-band by an order of magnitude. The maser uses a new type of photoetched slow-wave structure, integral with the ruby rod, especially suitable for millimeter-wave masers. It also employs a new type of built-in isolator configuration, which guarantees stable net gain of typically 30 dB over the tunable bandwidth, which is about 20 percent. Its phase stability, both short and long term, is excellent, making it highly suitable for use on an interferometer for radio astronomy.**

I. INTRODUCTION

MASERS have long been established as the lowest noise microwave amplifiers known, with present applications mainly in radio and radar astronomy as well as space communication receiver systems [1], [2]. Although laboratory masers have been operated up to 100 GHz, masers have not been in general use above 15 GHz, primarily because the limited applications of the higher frequencies did not warrant the development costs involved in adapting the laboratory maser versions for field use. Only the excellent Arams and Peyton maser, at 8 mm, was developed for this purpose [3], but was not intended for radio astronomy. More recently, a Russian ruby maser for use in radio astronomy at 8 mm has been described [4] as well as a Swedish design, which further developed the Arams–Peyton concept [5].

The discovery of a large number of interstellar molecules, most of which can be best detected at millimeter-wave frequencies, has given a new urgency to the development of low-noise millimeter-wave receivers for radio astronomy. The frequency range of the ruby maser reported here was chosen so as to incorporate the important inversion lines of ammonia (at $\geq$ 23.69 GHz) as well as the water vapor line at 22.235 GHz. The maser has also been used to observe or search for a large number of other molecules. The system noise temperature in a radio telescope using the maser is primarily determined by waveguide loss in the waveguide connecting the maser to the feed, and atmospheric thermal

Manuscript received October 30, 1975; revised June 28, 1976. The development of the *K*-band ruby maser was supported by the Office of Naval Research under Contract N00014-69-A-0200-1003.

K. S. Yngvesson is with the Department of Electrical and Computer Engineering, University of Massachusetts, Amherst, MA 01002.

A. C. Cheung, M. F. Chui, and C. H. Townes are with the Department of Physics, University of California, Berkeley, CA 94720.

A. G. Cardiasmenos is with the Department of Physics and Astronomy, University of Massachusetts, Amherst, MA 01002.

S. Y. Wang is with the Department of Electrical Engineering and Computer Sciences, University of California, Berkeley, CA 94720.

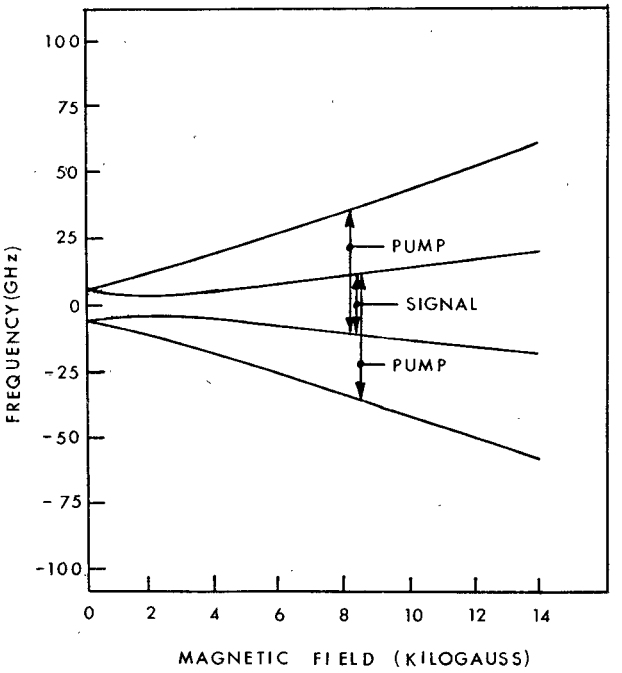

Fig. 1. Energy levels of ruby at the push–pull point ($\theta = 54.7°$).

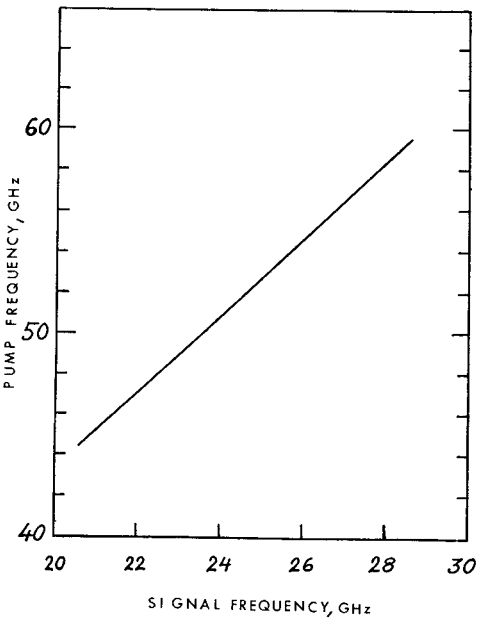

Fig. 2. Pump frequency for the maser as a function of the signal frequency.

noise. Single-sideband (SSB) system noise temperatures as low as 80 K have been obtained. The ruby maser described here uses a new type of comb structure and new isolator configuration to achieve 30-dB net gain over a tunable frequency range of about 20 percent.

II. Active Material

Although most earlier (laboratory) millimeter-wave masers have made use of rutile (with Cr^{3+} and Fe^{3+}), the present design uses ruby (Cr^{3+} in Al_2O_3) because ruby has some significant advantages over rutile. For instance, the quality of Czochralski-grown ruby presently available is superior to and more reproducible than the quality of commercial rutile. The lower dielectric constant ($\varepsilon_{\|} = 11$, $\varepsilon_{\perp} = 9$) compared with rutile also facilitates the microwave design problem.

Maser design data for ruby were readily available at X-band frequencies [6]–[8] and indicated that the optimum operating point is the so-called push–pull point, for which the externally applied dc magnetic field makes an angle of 54.7° with the c axis. The four ground-state energy levels of the Cr^{3+} ion in ruby are symmetric with respect to their "center of gravity" at this orientation of the magnetic field, as shown in Fig. 1. Thus it is possible to pump transitions 1–3 and 2–4 simultaneously while inverting transition 2–3. The pump frequency required is considerably lower than what would otherwise have to be used—an important consideration since millimeter-wave pump sources increase rapidly in price and decrease in life time as the frequency goes up. A signal frequency of 22 GHz, for example, requires a pump frequency of 47 GHz (Fig. 2). A slight disadvantage of the push–pull operation is that the orientation of the magnetic field is quite critical—it has to be held within 0.1–0.2° for optimum gain.

The electronic gain may be estimated from the expression [8]

$$G_{el} = -27.3S \frac{L}{\lambda_0} \eta\chi'' \text{ dB} \tag{1}$$

where

- $S \equiv$ slowing factor $= (c/v_g)$ (v_g is the group velocity of the wave);
- L active length of the maser;
- λ_0 free-space wavelength;
- η filling factor;
- χ'' imaginary part of the RF magnetic susceptibility at the signal transition frequency.

χ'' is given by

$$\chi'' = A(I(\Delta n_s)_0)N \frac{1}{\Delta f_l} \overline{|\sigma|^2} \tag{2}$$

where the constant A has the value

$$A \equiv 1.3 \cdot 10^{-18} \text{m}^3 \cdot \text{s}^{-1} \tag{3}$$

and

$$I \equiv \text{inversion ratio} = \frac{(\Delta n_s) \text{ with pump}}{(\Delta n_s)_0 \text{ without pump}};$$

- $(\Delta n_s \equiv n_2 - n_3$ is the fractional population difference for the signal transition);
- $N \equiv$ number of spins per cubic meter;
- $\Delta f_l \equiv$ linewidth in hertz (assuming the line shape to be Lorentzian);
- $\overline{|\sigma|^2} \equiv$ the square of the magnetic dipole matrix element (normalized so that $|\sigma|^2_{\max} = 2$ for an $S = 3/2$ system and circularly polarized RF fields) averaged over the microwave field distribution.

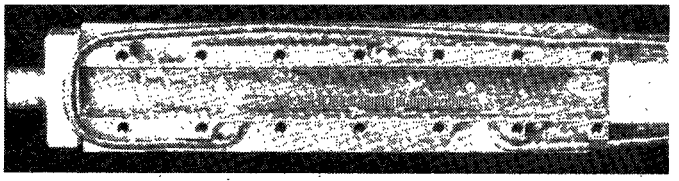

Fig. 3. Photograph of the maser base showing the ruby rod in the pump waveguide. Note that the isolator has been removed so that the slow-wave structure is clearly visible on the ruby.

Although η also depends on the material, i.e., the component of the matrix element which responds to the particular polarization of the field involved, χ'' incorporates the most important active material parameters. We may, in general, wish to maximize either χ'' or $\chi'' \cdot \Delta f_l$. The first choice will maximize the gain, while the second choice will essentially maximize the gain-bandwidth product (stagger tuning of the magnetic field would then be used to increase the bandwidth). In the present case, the bandwidth was adequate for spectral line work without stagger tuning of the magnetic field, and consequently it was sufficient to maximize χ''.

An inversion ratio of $I = -2$ was estimated by extrapolation of data taken at lower frequencies [7], and the measured value of -1.8 agrees quite well with the estimate. Further, $N = 2 \cdot 10^{25}\text{m}^{-3}$ for pink ruby, $(\Delta n_s) = 0.107$ at 2 K, $\overline{|\sigma|^2} = 1.6$, and $\Delta f_l = 60$ MHz so we find $h'' = -0.13$. This value can now be used to estimate the required product of $S \cdot L \cdot \eta$ for a given electronic gain. It will be seen later that $S = 25$ and $\eta = 0.2$ (a conservative estimate), so a length of ruby of the order 2–3 cm should provide sufficient gain. A similar estimate for Fe^{3+}-TiO_2 [5] results in $\chi'' \approx -0.05$, if $\Delta f_L = 200$ MHz is assumed. Thus this material yields somewhat smaller gain per unit length than ruby. However, the gain-bandwidth products, which are proportional to $\chi'' \cdot \Delta f_L$, should be very similar for the two materials.

In order to estimate the amount of pump power required to saturate the pump transitions, we first calculate the power that must be supplied in order to just barely break even with spin-lattice relaxation, given a certain number of spins and a spin-lattice relaxation time estimated to be of the order of 20 ms [9]. This power is about 3 mW. To provide enough margin for thorough saturation, about 50–100 mW should be adequate. The placement of the ruby in the pump waveguide is shown in Fig. 3. Using (2) and a geometric filling factor η_p, we can estimate the magnetic Q value for the pump

$$Q_{mp} = \frac{1}{\eta_p \cdot \chi_p''} \approx 5000. \tag{4}$$

The pump field is assumed to be perpendicular to the magnetic field (in the x direction), which gives the matrix element

$$|\sigma_{px}|^2 = 0.07 \tag{5}$$

which was used to arrive at (4). Under these conditions, only 1 percent of the pump power would be absorbed in a single passage of a 2-cm-long ruby rod, placed in a standard pump waveguide.

By reflecting the pump wave at the end of the ruby, we can increase the absorption of the pump wave, but it is still clear that pump saturation may be difficult to achieve. The primary reason for this is the very low transition probability. The latter is a general property of any $\Delta m_s > 1$ transition in an $S = 3/2$ system for magnetic fields such that $g\beta H > 2D$; this property tends to limit the highest frequency up to which a certain maser material may be used. Here $2D$ is the zero-field splitting of the ground-state doublet, g is the effective g factor, and β is the Bohr magneton. For ruby this limit occurs at about 40–50 GHz. In the present maser, the pump saturation is sufficiently good so that the gain is acceptably stable, but the gain stability could still be improved somewhat, and further work is in progress in this direction.

III. Slow-Wave Structure

A new type of periodic slow-wave structure has been developed, which is particularly suitable for millimeter-wave traveling-wave masers (TWM's), since it depends on integrated circuit techniques for meeting the high requirements on precision in fabricating the small circuit. The ruby rod is cut and lapped to correct dimensions, whereupon a 200-Å-thick layer of chromium is evaporated on three sides of the rod, immediately followed by about 0.5 μm of evaporated copper. One of the sides is evaporated through a mask to form a comb structure. The adhesion of the film is improved by a heat treatment in a hydrogen atmosphere. The thickness of the copper film is increased to 2.5 μm by electroplating.

Earlier work by Loriou and Jaouen [10] had utilized photoetching in the fabrication of the comb structure for a 4-GHz TWM. Their design requires assembling two ruby rods, one with a comb, and another one with metallization on three sides but no comb, into a symmetric package resembling the comb structure of DeGrasse *et al.* [11], extensively used in centimeter-wave ruby TWM's. Although high slowing can be obtained, the assembly of such a structure for a millimeter-wave maser would be quite difficult. Instead, we have developed an asymmetric structure which can be made in the manner just described (for similar reasons, asymmetric microstrips are preferred in microwave integrated circuits to symmetric striplines). The new structure was developed by the use of models operating at about 600 and 4600 MHz, respectively, using Stycast and alumina dielectrics (both with $\varepsilon_r \simeq 10$) to simulate the dielectric constant of ruby. The 600-MHz model used copper tape for the comb, while the 4600-MHz comb was evaporated and photoetched. We investigated both symmetric and asymmetric structures to compare their advantages. The dimensions of a structure are defined in Fig. 4.

The dispersion curves of the models were obtained by observing the resonances due to reflections at each end, and the slowing factors were then calculated as a function of frequency. Suitable coupling elements were developed empirically. The bandwidth of the structure determines the

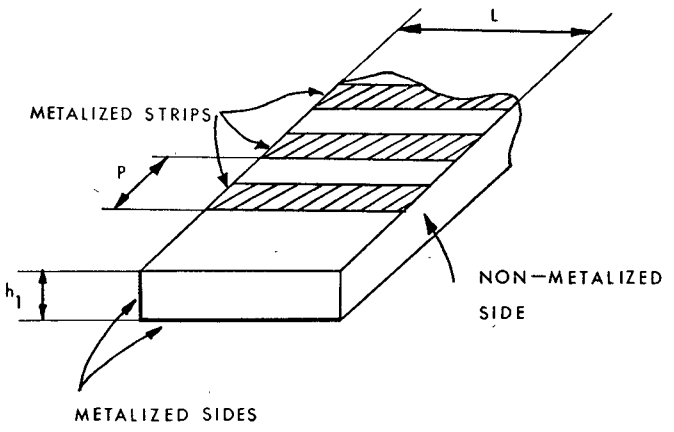

Fig. 4. Basic dimensions of the slow-wave structure.

tunable bandwidth of the maser and for practical purposes we may define this tunable bandwidth (Δf) as the difference between the frequencies for which $S = 2 \cdot S_{min}$.

It was first established that the minimum slowing factor and the bandwidth are essentially independent of the pitch: In two 4600-MHz symmetric structures, the slowing remained the same while the bandwidth increased slightly from about 20 to 22 percent, when the pitch (P/L in Fig. 4) was decreased by a factor of 2. The ratio P/L went from 0.85 to 0.43 (L is the length of a strip). In all later structures, P/L was in the range 0.33–0.42. Similarly, changing the relative strip widths and their spacings had no major effect. The parameter h_1/L, i.e., the normalized thickness of the dielectric, is largely the one which controls the properties of both symmetric and asymmetric structures. As can be seen from Fig. 5, the slowing factor rises very rapidly with decreasing thickness, particularly for the symmetric structure. The data for the latter are consistent with those of Loriou and Jauoen [10]. Two variations of the asymmetric structure were investigated, one with a strip length equal to the width of the dielectric and another where the strips do not reach the edge of the dielectric. The former configuration yields $S_{min} = 25$ at $h_1/L = 0.36$, with a relative bandwidth of 26 percent, while the latter structure has $S_{min} = 14$ and $\Delta f/f_0 = 41$ percent (f_0 is the center frequency). The structure with strips reaching the edge was chosen because it is easier to fabricate and yields the estimated slowing-factor requirement. For future development, one should note that the very large bandwidth of 41 percent for the second type of asymmetric structure is very attractive, since it is conceivable in an optimized maser to obtain sufficient gain even with $S = 14$.

The usable relative bandwidths of the structures are also compared in Fig. 5. It can be seen that the symmetric structure pays for its higher slowing capability (at low h_1/L) with a narrower bandwidth. The bandwidth of the asymmetric model is typically twice that of the symmetric one and has a somewhat weaker dependence on h_1/L.

van Dijk *et al.* [12] have calculated the dispersion curves and filling factors of our type of structure by approximating the comb with a sheath conducting in the direction of the strips but not perpendicular thereto. This approximation should describe the behavior well for slow-wave wavelengths

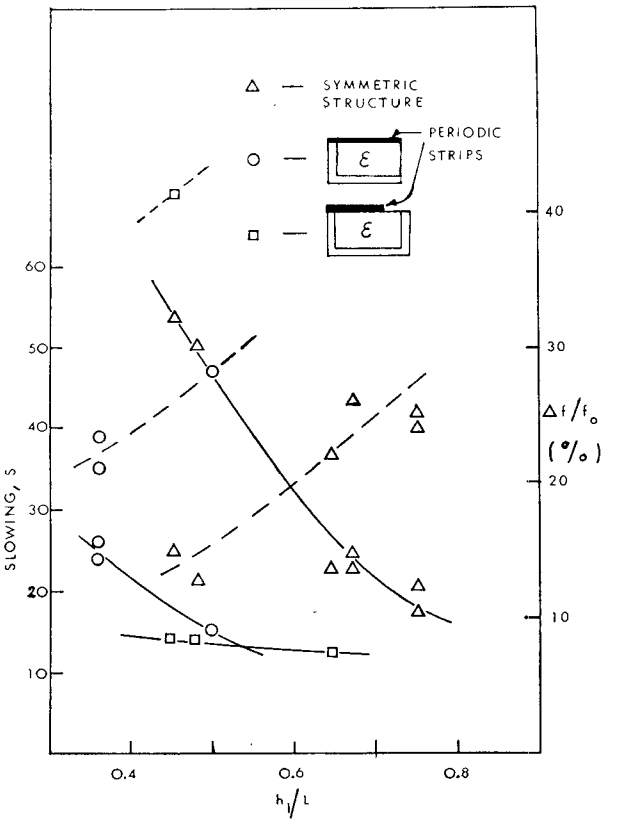

Fig. 5. Slowing factor (S, full curves) and relative bandwidth ($\Delta f/f_0$, broken curves) as a function of h_1/L for three different types of structures.

long compared to the pitch. In agreement with our data, they find that the slowing increases with decreasing h_1/L If the approximation is valid, one further expects S to be independent of P, as observed. The structure bandwidth is predicted by van Dijk *et al.* [12] to be independent of h_1/L. In our data, Δf does depend on h_1/L, but Δf is not likely to be as well predicted by the theory, since wavelength and pitch become comparable in the upper portion of the passband. A major advantage of the new slow-wave structure is the large volume filling factor, which is predicted to be 1 at lower cutoff, smoothly decreasing to 1/2 at upper cutoff.

We also investigated the polarization of the fields above the structure, both by a small loop probe and by incorporating YIG in the 4600-MHz structure and then measuring the resonant loss in a magnetic field. The best circular polarization is obtained at the top of an alumina rod, with a width of about 40 percent of the width of the ruby, placed near the shorted end of the strips. The additional dielectric loading increases S by about 10 percent, while shifting the passband downward in frequency by a somewhat smaller percentage. In a later section, we will discuss how the isolator was incorporated in the alumina rod.

The best coupling to the asymmetric structure was obtained by using a coupling strip of the same width and separation as used in the comb, and shorting the far end of the coupling strip to the ground plane. Alternatively, one may couple the structure from the open end, using a coupling strip of the same dimensions, which ends in an open

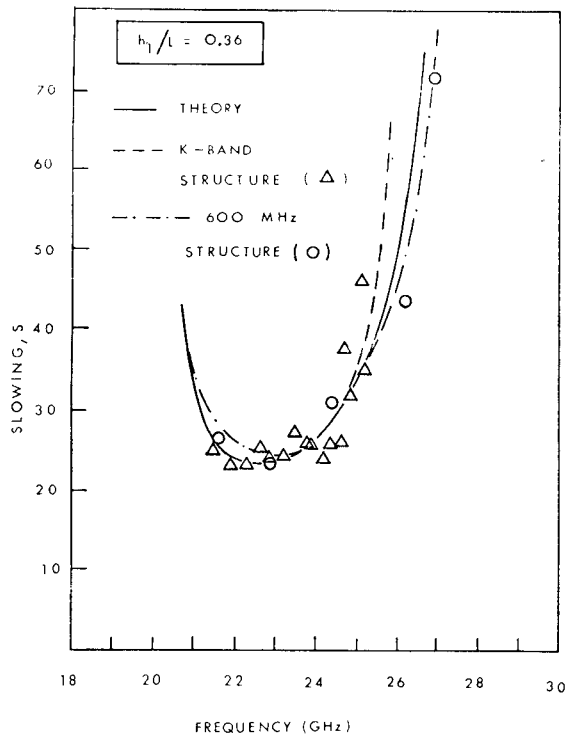

Fig. 6. Slowing factor (S) as a function of frequency for two structures (see text). The theoretical curve was calculated by Kollberg and Lewin.

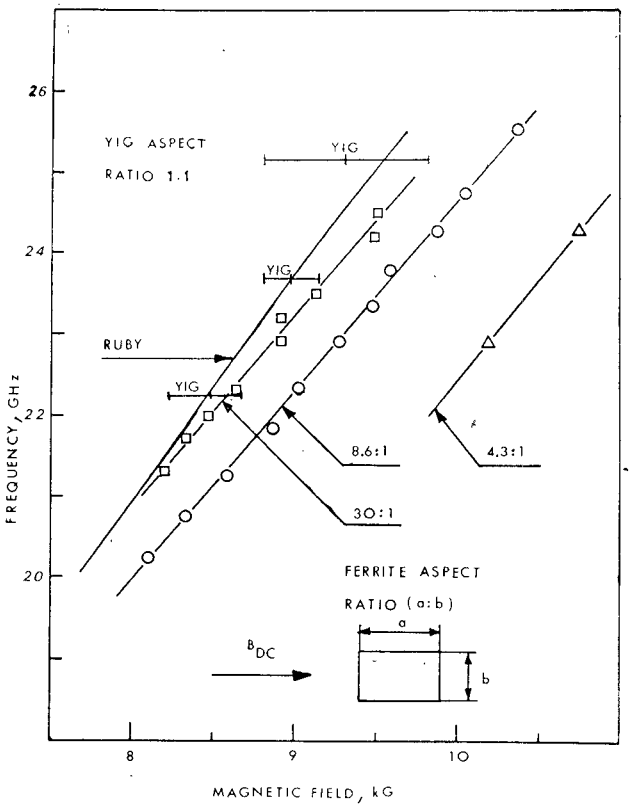

Fig. 7. Tracking curves for the ruby resonance and two different isolator materials: TT2-113 ferrite and YIG. For the YIG, the linewidth is also indicated.

circuit. The coupling was developed using standard 50-Ω cables in the 600-MHz model, while a semirigid coax of outer diameter 0.114 cm was used at K band. The ripple in the transmission curve of a typical K-band unit was about 2 dB.

Finally, we show the measured slowing curve versus frequency for the 600-MHz model and the actual scaled ruby comb structure at K band (Fig. 6). In order to obtain the latter curve, we measured the phase shift through the K-band structure by an interference method in which the input power was split in two paths, one incorporating the comb, the other an attenuator, and then recombining and detecting the sum of the two waves. The dispersion curve was then derived from the observed interference pattern, a method often used for structures with appreciable attenuation. Since the theory neglects any fringe fields, it is reasonable to shift the calculated dispersion curve to the same lower cutoff frequency as the measured one. It then agrees very well with the measured frequency-scaled dispersion curve for the 600-MHz model. The measured slowing of the K-band ruby structure, shown in the same figure, also agrees well except in the region near upper cutoff, where it rises more steeply. In this frequency range, the dispersion curve is expected to be very sensitive to any small difference between the model and the actual K-band structure, such as the anisotropic dielectric constant of ruby. The actual usable bandwidth is somewhat smaller than predicted by the model (21 versus 23 percent), but overall the agreement is completely satisfactory and shows the usefulness of the method of design by frequency scaling.

The type of structure we have investigated should also be useful for filter applications in microstrip integrated circuits. We found that it is easy to couple to a 50-Ω microstrip as well as to the coax we usually used in the maser structures. Filters would be made most easily with $\lambda/2$ long strips, for which no shorting plane would be needed.

IV. Isolator

The ferrite isolator is designed in such a way that the loop gain for a wave reflected between the two ends of the slow-wave structure is much less than one for all frequencies, resulting in a stable nonregenerative amplifier [8]. Since the maser gain in the reverse direction is about one-half (in decibels) of the gain in the forward direction, the isolator needs to provide a reverse attenuation which is typically greater than the net gain in the forward direction. As in other TWM's, the isolator consists of a bar of ferromagnetic material, placed in a position where the slow-wave structure produces circularly polarized microwave magnetic fields of opposite sense for the two possible directions of propagation along the structure.

We first investigated a rather special ferrite, aluminum-doped nickel ferrite (Transtech TT2-113). The aluminum doping in this material is such that the two magnetic sublattices have just passed the compensation point (at which they are equal). The resulting resonance exhibits an effective g value which is less than 2 [13]. We tried several different shapes of this material, and the resonance frequency versus magnetic-field curves are compared with the corresponding curve for the push–pull point in ruby in Fig. 7. The shapes are characterized by the aspect ratios defined in this figure. Satisfactory tracking of the ruby and ferrite curves was

obtained for the largest aspect ratio (30:1), but unfortunately this ferrite was so thin that the reverse attenuation was much too small to be useful. We nevertheless review these data here since this material in sufficient thickness would track the ruby push–pull point at around 15 GHz and thus may be useful in designing a ruby TWM at that frequency. As far as we know, this is the first time that ferrites with g value not close to 2 have been investigated for use in masers. The effective g value for TT2-113 was found to be 1.6 (at liquid helium temperature).

A bar of roughly square cross section of any ferrite with $g_{\text{eff}} \approx 2$ also tracks the ruby line, as shown in Fig. 7. The square shape caused considerably more distortion of the dc field in the ruby than the flat bars of TT2-113 described previously. For example, a bar of YIG of sufficient size to give the required reverse attenuation produced broadening of the ruby line from its natural linewidth of 23 G to 50–100 G, decreasing the gain by the same factor. The solution found for this problem was to add a second bar of TT2-113, parallel to and at some distance from the YIG. The cross section of the second bar was chosen to match the magnetization of the YIG. Since TT2-113 has a lower effective g value than YIG, it has its resonance at a much higher field, and does not have a perturbing influence on the resonance of the YIG. An isolator rod in this configuration did not perturb the ruby linewidth noticeably. Typical values of reverse attenuation are 50–70 dB, with forward attenuation of about 2 dB. Thus the maser is unconditionally stable.

V. Superconducting Magnet

The superconducting magnet design was developed from that of Hentley [14]. The magnet winding is closed at the bottom, while at the top it is separated into two halves to allow insertion of the maser. The cross section of the magnet is similar to that of Hentley, with an air gap along the field of 2 cm and a width of about 1 cm. Since the ruby rod has a very small cross section, the crucial homogeneity is along the axis of the magnet. This was measured with a magnetoresistive element. A typical field required for operation of the maser is 8–10 kG, and at this level the magnetic field changes by less than 10 G over a length of 5 cm. Since the intrinsic ruby linewidth is 23 G, the inhomogeneous broadening due to the magnet should be negligible for ruby rods up to 5 cm long. The current required is less than 10 A, and a conventional persistant mode switch is used to obtain a stable magnetic field after it has been adjusted for maximum maser gain.

VI. Microwave Circuitry

The ruby rod with its evaporated slow-wave structure is soldered to the bottom of the pump waveguide, which is milled from a piece of gold-plated molybdenum, chosen so as to match the thermal contraction of ruby from room temperature to liquid helium temperature. A typical pump source is a Varian reflex klystron with an output of 100 mW over a 6-GHz tunable range, corresponding to a K-band signal bandwidth of 3 GHz. Two pump klystrons are thus required to cover the tunable band of the maser. Typical gain increases of 3 dB were obtained when the klystron frequency was square-wave modulated at about 50 kHz. No special effort has been made to improve the coupling of pump power into the ruby, aside from tapering that end of the ruby rod which faces the incoming pump wave. The pump waveguide is terminated by a fixed short which reflects the pump wave back past the ruby (see Fig. 3). Copper-plated stainless-steel waveguides are used for the input and output of the maser as well as the pump. At the maser base, the input and output waveguides make a transition to miniature coaxial cables. The center conductors of the cables are soldered to the comb coupling strips, while the outer conductors fit though a hole in the pump waveguide wall, to which they are joined by soldering. Low-pass filters in the signal waveguides prevent the pump from leaking into either the antenna feed or the mixer receiver which follows the maser. This precaution eliminates a potential cause of gain variations.

The ruby base is finally located with respect to the magnet by means of a low-temperature bearing arrangement, which allows orientation of the ruby to the push–pull angle. The photograph in Fig. 8 shows the completed maser amplifier, including superconducting magnet, pump and control circuitry, and the dewar.

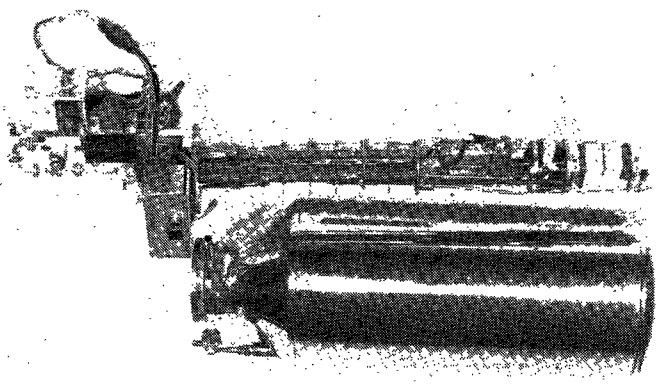

Fig. 8. Photograph of the completed maser.

TABLE I
Maser Characteristics

Length	Passband	Passive Loss	4°K Gain	4°K BW	4°K Pump Power	1.5°K Gain	1.5°K BW	1.5°K Pump Power
(cm)	(GHz)	(dB)	(dB)	(MHz)	(mW)	(dB)	(MHz)	(mW)
2	23.8 to 26.5	8	15	40	200	30-40	30-40	50
3	18.0 to 24.2	6-10	23	30	100	30-40	30-50	30
4	21.9 to 26.0	20	-	-	-	25	25	100

VII. Performance

Ruby lengths of 2, 3, and 4 cm were tested. All three produced working devices, the characteristics of which are shown in Table I. Variations in the input–output coupling to the ruby produced the differences in insertion loss. The longest (4 cm) ruby produced poor results. This was attributed to the last section of ruby which did not become

inverted, resulting in loss instead of gain. This is further evident from reversing the input and output terminals so that the input is now further from the pump signal. The input noise temperature of the device then increased sharply to over 150 K. The optimal length is therefore empirically determined to be about 3 cm since this allows sufficient gain at 4.2 K and renders vacuum pumping on the helium unnecessary.

The bandwidth of the device can be increased further by staggering the magnetic field and increasing the pump power at 1.5 K operation. A factor of 2 increase in bandwidth is easily achieved with a magnetic-field inhomogeneity of about 10 G and a 50-percent increase in pump power. At the pump power levels required for 1.5 K operation, presently available solid-state devices have been used in the laboratory. These will greatly simplify field operation.

The phase stability of one maser was tested by monitoring the phase at the maser output, with the maser tuned up to high gain at a given frequency. Short-term ($\sim$0.1-s) phase fluctuations were less than 0.2°, and the long-term drift was measured to be 9°/h, mostly from pump klystron power supply drift. Since integration times in radio astronomy interferometry are typically of the order of minutes, the phase stability of the maser is more than adequate for this type of work, which will be one of the most interesting applications of this type of low-noise receiver in the future.

We have field tested versions of the maser design described here in two single-dish applications, in particular in the University of California, Berkeley, 20-ft millimeter-wave telescope at Hat Creek, CA, and in the Naval Research Laboratory 85-ft dish at Maryland Point, MD. A similar maser has also been assembled and tested by two of us (Yngvesson and Cardiasmenos) in cooperation with personnel at the NEROC Haystack Observatory and successfully operated in the Haystack 120-ft telescope [15]. SSB system noise temperatures as low as 80 K have been obtained in these installations. As a comparison, a typical uncooled parametric amplifier yields a SSB system noise temperature almost an order of magnitude greater [16], while a recent cooled parametric amplifier has provided a system noise temperature about twice that of the present maser [17]. In comparing the system noise temperatures, one should remember than the observing time required to achieve a given signal-to-noise ratio is proportional to the square of the system noise temperature. Thus a reduction in noise temperature by a factor of 2 saves a factor of 4 in observing time.

ACKNOWLEDGMENT

The authors wish to thank the Radio Astronomy Branch of the Naval Research Laboratory for their advice and cooperation. They also wish to thank E. Kollberg and T. Lewin of Chalmers University of Technology for calculating the theoretical curve in Fig. 6, and D. Thornton for the design of the waveguide–coax transitions.

REFERENCES

[1] E. L. Kollberg, "A traveling-wave maser system for radio astronomy," *Proc IEEE*, vol. 61, pp. 1323–1329, Sept. 1973.
[2] M. S. Reid, R. C. Clauss, D. A. Bathker, and C. T. Stelzried, "Low-noise microwave receiving systems in a worldwide network of large antennas," *Proc. IEEE*, vol. 61, pp. 1330–1335, Sept. 1973.
[3] F. Arams and B. Peyton, "Eight-millimeter traveling wave maser and maser-radiometer system," *Proc. IEEE*, vol. 53, pp. 12–23, Jan. 1965.
[4] V. I. Zagatin, G. S. Miserzhnikov, and V. B. Shteynshleyger, "Ruby maser operating in the 8 mm range," *Radio Eng. El. Phys.*, vol. 12, pp. 501–502, Mar. 1967.
[5] A. G. Cardiasmenos, K. S. Yngvesson, and E. L. Kollberg, "Maser amplifiers for 20–24 GHz using ruby and iron-doped rutile," IEEE International Microwave Symposium, Boulder, Colorado, June 1973.
[6] E. O. Schulz-DuBois, "Paramagnetic spectra of substituted sapphires—Part I: Ruby," *Bell Syst. Techn. J.*, vol. 38, pp. 271–290, Jan. 1959.
[7] R. C. Clauss, *JPL Space Programs Summary 37–61*, vol. III, p. 90, 1970.
[8] A. E. Siegman, *Microwave Solid State Masers*, New York: McGraw-Hill, 1964.
[9] G. Brown and J. S. Thorp, "The measurement of spin-lattice relaxation times at very low power levels," *Brit. J. Appl. Phys.*, vol. 18, pp. 1423–1431, Oct. 1967.
[10] B. Loriou and J. L. Jaouen, "C-band traveling-wave maser using a slow-wave structure printed on ruby," *Proc. IEEE* (Lett.), vol. 55, pp. 461–462, Mar. 1967.
[11] R. W. DeGrasse, E. O. Schulz-DuBois, and H. E. D. Scovil, "The three-level solid state traveling-wave maser," *Bell Syst. Techn. J.*, vol. 38, pp. 305–334, Mar. 1959.
[12] M. H. H. van Dijk, C. E. Hagstrom, and E. L. Kollberg, "The dielectrically loaded 'easitron' circuit as a slow-wave structure for traveling-wave maser applications," *Int. J. Electronics*, vol. 36, pp. 495–506, Apr. 1974.
[13] W. H. von Aulock (Ed.), *Handbook of Microwave Ferrite Materials*, New York: Academic Press, 1965, p. 399.
[14] E. L. Hentley, "Superconducting magnet for an 8 mm traveling-wave maser," *Cryogenics*, vol. 7, pp. 33–35, Feb. 1967.
[15] P. B. Sebring, "New maser at Haystack," *Science*, vol. 179, p. 128, Jan. 1973. Also L. Raineville, J. C. Carter, S. H. Zisk, private communication.
[16] D. Buhl, L. Snyder, and J. Edrich, "An interstellar emission line from HNCO at 1.4 cm," *Astrophys. J.*, vol. 177, pp. 625–628, Nov. 1972.
[17] N. Broten, private communication, 1975.